Laggera alata attenuates LPS-induced systemic inflammation and hepatic-pulmonary injury by regulating PINK1/Parkin-associated mitophagy and macrophage polarization

JIANGCUN WEI[1,2], WEN ZHONG[1], GUANGYUN ZHOU[2], MINGTAO HUANG[2], XIAODONG HUANG[2] and JING LIANG[3]

[1]Zhuang and Yao Medicine Preparation Center, International Zhuang Medicine Hospital Affiliated to Guangxi University of Chinese Medicine, Nanning, Guangxi 530201, P.R. China; [2]Department of Pharmacy, Guangxi University of Chinese Medicine, Nanning, Guangxi 530200, P.R. China; [3]Department of Reproductive Medicine, International Zhuang Medicine Hospital Affiliated to Guangxi University of Chinese Medicine, Nanning, Guangxi 530201, P.R. China

Received December 8, 2025; Accepted May 27, 2026

DOI: 10.3892/mmr.2026.13956

Abstract. *Laggera alata* is a traditional medicinal herb used for inflammatory and infectious diseases, but its mechanisms against endotoxin-induced systemic inflammation remain unclear. The present study investigated the protective effects of total phenolics from *Laggera alata* (TPLA) on lipopolysaccharide (LPS)-induced inflammatory injury and explored the involvement of PTEN-induced putative kinase 1 (PINK1)/Parkin-associated mitophagy and macrophage polarization. LPS-induced inflammatory models were established in RAW264.7 macrophages and C57BL/6 mice. Cell viability, apoptosis, mitochondrial membrane potential (MMP), cytokine production, macrophage polarization and mitophagy-related protein expression were evaluated. Mdivi-1 was used to assess the involvement of mitophagy-related signaling. *In vivo*, core body temperature, serum cytokines, and lung and liver histopathology were examined. TPLA improved the viability of LPS-stimulated macrophages, reduced apoptosis, restored MMP, decreased p62 expression, and increased PINK1, Parkin and the LC3-II/LC3-I ratio. TPLA also suppressed M1-associated indicators, including inducible nitric oxide synthase, IL-12 and CD80/CD86, while enhancing M2-associated indicators, including arginase 1, IL-10 and CD206/CD163. In addition, TPLA reduced IL-1β, IL-6 and TNF-α release. Mdivi-1 partially reversed the effects of high-dose TPLA on mitophagy-related protein expression and macrophage polarization. In LPS-challenged mice, TPLA alleviated hypothermia, reduced systemic cytokine levels, and attenuated hepatic and pulmonary injury. These findings suggest that TPLA protects against LPS-induced systemic inflammation and hepatic-pulmonary injury by modulating PINK1/Parkin-associated mitophagy-related signaling and macrophage polarization.

Introduction

Sepsis is a life-threatening syndrome defined by organ dysfunction arising from a dysregulated host response to infection, with up to 60% of patients progressing to acute kidney injury (AKI) (1). Its pathogenesis is multifactorial, involving excessive immune activation, cytokine storms and microvascular dysfunction (2). Despite progress in supportive care, sepsis remains a major clinical challenge, contributing to ~11 million deaths worldwide annually, and often results in poor outcomes for survivors (3). Current treatments primarily rely on early recognition and non-specific supportive interventions, such as broad-spectrum antibiotics, fluid resuscitation and hemodynamic stabilization (4). However, no effective targeted pharmacotherapies exist, and present strategies remain largely symptomatic and insufficient (3).

Traditional Chinese medicine (TCM) offers therapeutic benefits through multi-component, multi-pathway and multi-target mechanisms and is considered a potential complementary strategy for the management of sepsis-related inflammatory disorders (5). *Laggera alata (D. Don) Sch. Bip. ex Oliv*, a member of the Asteraceae family, is native to eastern,

Correspondence to: Dr Xiaodong Huang, Department of Pharmacy, Guangxi University of Chinese Medicine, 13 Wuhe Avenue, Qingxiu, Nanning, Guangxi 530200, P.R. China
E-mail: zgy155623@163.com

Dr Jing Liang, Department of Reproductive Medicine, International Zhuang Medicine Hospital Affiliated to Guangxi University of Traditional Chinese Medicine, 8 Qiuyue Road, Liangqing, Nanning, Guangxi 530201, P.R. China
E-mail: ljgxszk_2023@126.com

Abbreviations: TPLA, total phenolics from *Laggera alata*; LPS, lipopolysaccharide; iNOS, inducible nitric oxide synthase; Arg1, arginase 1; PINK1, PTEN-induced putative kinase 1

Key words: LPS-induced systemic inflammation, TPLA, PINK1/Parkin, mitophagy, macrophage polarization

southeastern and southwestern China and has been traditionally used in TCM for effects traditionally described as dispelling wind, eliminating dampness and detoxification (6). As a traditional Chinese medicinal herb, *Laggera alata* has long been used in Chinese folk medicine to treat various disorders and has been reported to exhibit antibacterial, anti-inflammatory and antipyretic activities (7). Traditionally, *Laggera alata* has been commonly used for the treatment of upper respiratory tract infections, influenza, parotitis and recurrent herpes viral infections, with its extracts showing notable anti-inflammatory and antiviral activities (8). Additionally, this plant is frequently employed to eliminate phlegm and treat bronchitis and jaundice, which is closely related to its rich essential oil content. These essential oils are mainly composed of oxygenated monoterpenes and sesquiterpenes, among which the aromatic ether 2,5-dimethoxy-p-cymene is one of the major active constituents (9). Modern pharmacological studies have shown that extracts of *Laggera alata* possess anti-inflammatory properties and show protective effects in various disease models, including carbon tetrachloride-induced hepatic fibrosis (10), collagen-induced rheumatoid arthritis (11) and sepsis-associated AKI (12). However, the molecular mechanisms underlying its effects in endotoxin-induced systemic inflammation remain poorly understood.

The authors' previous research demonstrated that total phenolics extracted from *Laggera alata* (TPLA) attenuated inflammation in a rheumatoid arthritis model by suppressing M1 macrophage polarization (11). Among the key drivers of multi-organ dysfunction in sepsis is mitochondrial impairment, especially in the kidneys (13). Mitophagy, an essential mitochondrial quality-control process that selectively eliminates damaged or superfluous mitochondria, has recently been recognized as a critical regulator of mitochondrial homeostasis, immune regulation and disease progression (14-16). Among the currently identified mitophagy pathways, the PTEN-induced putative kinase 1 (PINK1)/Parkin-dependent pathway remains one of the best-characterized mechanisms, in which PINK1 accumulates on damaged mitochondria and recruits Parkin to initiate mitochondrial ubiquitination and autophagic clearance (16). Recent evidence further indicates that mitochondrial dysfunction, impaired mitophagy, excessive mitochondrial reactive oxygen species (ROS) production and altered mitochondrial metabolism are closely associated with macrophage polarization imbalance and immune dysregulation during sepsis (17,18). Moreover, activation of the PINK1/Parkin pathway has been shown to mitigate renal injury and improve outcomes in AKI models (19). In particular, recent studies have linked PINK1/Parkin-mediated mitophagy to macrophage phenotype remodeling, suggesting that mitophagy may serve as a mechanistic bridge between mitochondrial quality control and inflammatory resolution (20,21). While mitophagy has emerged as a key mechanism in sepsis pathophysiology, the potential role of TPLA in modulating PINK1/Parkin-associated mitophagy and immune regulation has not yet been investigated. The present study aimed to elucidate the mechanisms by which TPLA alleviates LPS-induced systemic inflammation and organ injury, with a focus on PINK1/Parkin-associated mitophagy and macrophage polarization.

Materials and methods

Preparation of TPLA. Plant material was collected on November 29, 2019, from Sanfang Reservoir (Longxu, Cangwu, Guangxi, China). The voucher specimen (collection no. 450421191129020LY) was deposited in the Herbarium of Guangxi Institute of Botany (IBK) under voucher number IBK00430105. The specimen was identified by Yusong Huang on October 24, 2020, as *Laggera alata (D. Don) Sch. Bip. ex Oliv*, a species belonging to the genus *Laggera* of the family Asteraceae. The whole plant was used for extraction. The plant name was verified against The Plant List (http://www.theplantlist.org). TPLA was extracted according to previously published protocols (11). Dried *Laggera alata* herb (10 kg) was ground into coarse powder and extracted twice by reflux with 95% ethanol at ~84˚C, using solvent-to-material ratios of 12:1 and 8:1 (L/kg) for 1.5 and 1 h, respectively. The combined extracts were filtered, concentrated under reduced pressure using a rotary evaporator, and subsequently dried in a 65˚C water bath. The yield of TPLA (total phenolics: 13.52%) was 2.156 kg, with an extraction efficiency of 21.56%. The extract was sealed and stored in a dry environment. For experimental use, an accurately weighed amount of TPLA powder was dissolved in distilled water and diluted to the required concentration immediately before use.

Cell culture and treatment. The mouse macrophage cell line RAW264.7 (cat. no. CL-0190; Wuhan Pricella Biotechnology Co., Ltd.) was cultured in high-glucose Dulbecco's Modified Eagle Medium (DMEM; cat. no. E600003; Sangon Biotech Co., Ltd.) supplemented with 10% fetal bovine serum (FBS; Guangzhou Yunoer Biotechnology Co., Ltd.) and 1% penicillin-streptomycin (cat. no. P1400; Beijing Solarbio Science & Technology Co., Ltd.) at 37˚C in a 5% CO_2 incubator. Cells were tested and confirmed to be mycoplasma-free and authenticated by short tandem repeat (STR) profiling (Wuhan Pricella Biotechnology Co., Ltd.). Cells at 80-90% confluence were used for experiments. To establish an *in vitro* LPS model group, cells were treated with 1 μg/ml lipopolysaccharide (LPS; cat. no. L2630; MilliporeSigma) for 24 h (22), followed by treatment with TPLA at low (10 μg/ml), medium (50 μg/ml) and high (100 μg/ml) concentrations or dexamethasone (DEX; 10 μM; cat. no. D4902; MilliporeSigma). The control group received no treatment. For mitophagy inhibition experiments, cells were additionally assigned to the LPS, LPS + TPLA-high, and LPS + TPLA-high + Mdivi-1 groups. Mdivi-1 (10 μM; cat. no. M0199; Sigma-Aldrich; Merck KGaA) was added 1 h before TPLA-high treatment. Mitophagy-related protein expression was subsequently evaluated by western blotting. In the Mdivi-1 inhibition experiment, macrophage polarization was further assessed by flow cytometry using CD80/CD86 as M1-associated markers and CD206/CD163 as M2-associated markers.

Enzyme-linked immunosorbent assay (ELISA). Levels of IL-1β (cat. no. MLB00C-1; R&D Systems, Inc.), IL-6 (cat. no. BMS603-2), TNF-α (cat. no. BMS607-3TEN), IL-1α (cat. no. 900-K82K), IL-4 (cat. no. 88-7044-88) and IL-10 (cat. no. 88-7105-88; all from Thermo Fisher Scientific, Inc.) were quantified using ELISA kits. Samples were added

to 96-well plates pre-coated with capture antibodies and incubated for 2 h at 37˚C. After washing, biotin-conjugated detection antibodies were added and incubated for 1 h at 37˚C, after which the substrate solution (cat. no. A8043; Thermo Fisher Scientific, Inc.) was added for color development. Absorbance was measured at 450 nm using a microplate reader (Varioskan™ LUX; Thermo Fisher Scientific, Inc.), and concentrations were calculated from standard curves.

JC-1 staining for mitochondrial membrane potential (MMP). MMP was assessed using JC-1 dye (cat. no. C2006; Beyotime Institute of Biotechnology). After 24 h of treatment, cells were washed with PBS and incubated with 5 μM JC-1 at 37˚C for 30 min in the dark. After staining, cells were washed with JC-1 buffer and immediately analyzed by flow cytometry (Accuri C6; BD Biosciences). Fluorescence signals were collected in the FL1-H (green, JC-1 monomers, 530±15 nm) and FL2-H (red, JC-1 aggregates, 585±20 nm) channels under logarithmic scaling. At least 10,000 events were recorded per sample. The red/green fluorescence ratio was calculated to represent MMP, where red fluorescence indicates polarized mitochondria and green fluorescence indicates depolarization. Data were analyzed using FlowJo software (v10.8; BD Biosciences).

Cell Counting Kit-8 (CCK-8) assay. RAW264.7 cells were seeded at 6x10^4 cell/ml (200 μl per well) in 96-well plates and treated according to group allocation. After 24 h of treatment, 20 μl of CCK-8 reagent (cat. no. CK04; Dojindo Laboratories, Inc.) was added to each well and incubated for 2-4 h at 37˚C. Absorbance was then measured at 450 nm using a microplate reader (Synergy H1; BioTek; Agilent Technologies, Inc.).

Flow cytometric analysis of apoptosis. Apoptosis was evaluated using the Annexin V-FITC/PI Apoptosis Detection Kit (cat. no. A211-01; Vazyme Biotech Co., Ltd.) following the manufacturer's instructions. After washing with PBS (cat. no. E600003; Sangon Biotech Co., Ltd.), cells were digested with 0.25% trypsin (cat. no. C0201; Beyotime Institute of Biotechnology) without EDTA, resuspended in 1X binding buffer, and incubated with 5 μl Annexin V-FITC and 5 μl propidium iodide (PI) for 15 min at room temperature in the dark. Samples were immediately analyzed by flow cytometry (Accuri C6; BD Biosciences). Fluorescence was detected using the FL1-H (FITC, 530±15 nm) and FL3-H (PI, >670 nm) channels under logarithmic scaling. Compensation was applied using single-stained controls. At least 10,000 events were acquired per sample, and debris and doublets were excluded by forward- and side-scatter gating. Early and late apoptotic cell percentages were calculated using FlowJo software (v10.8; BD Biosciences).

Western blotting. RAW264.7 cells were lysed in RIPA buffer (cat. no. P0013B; Beyotime Institute of Biotechnology) after washing with PBS, and lysates were centrifuged at 12,000 x g for 15 min at 4˚C to collect supernatants. Protein concentration was determined using a BCA protein assay kit (cat. no. P0012; Beyotime Biotechnology) according to the manufacturer's instructions. Equal protein amounts (30 μg) were resolved on 10% gels using SDS-PAGE together with a pre-stained protein marker (cat. no. G2086; Wuhan Servicebio Technology Co., Ltd.), followed by transfer onto PVDF membranes (MilliporeSigma). Membranes were blocked with 5% non-fat milk in TBST containing 0.1% Tween-20 for 1 h at room temperature and then incubated with primary antibodies overnight at 4˚C: LC3B rabbit monoclonal antibody (1:2,000; cat. no. ab192890; Abcam), p62 rabbit polyclonal antibody (1:10,000; cat. no. ab109012; Abcam), Parkin rabbit polyclonal antibody (1:1,000; cat. no. GB11596; Wuhan Servicebio Technology Co., Ltd.), PINK1 rabbit polyclonal antibody (1:500; cat. no. GB114934; Wuhan Servicebio Technology Co., Ltd.) and GAPDH rabbit polyclonal antibody (1:2,500; cat. no. ab9485; Abcam). After incubation with horseradish peroxidase (HRP)-conjugated goat anti-rabbit IgG secondary antibody (1:10,000; cat. no. ab6721; Abcam), chemiluminescent signals were detected on X-ray films using ECL substrate (Thermo Fisher Scientific, Inc.). Band intensities were analyzed with ImageJ software (v1.80; National Institutes of Health).

Reverse transcription-quantitative PCR (RT-qPCR). Total RNA was extracted using RNAiso Plus reagent (cat. no. 9109; Takara Bio, Inc.), and RNA purity and concentration were determined using a NanoDrop spectrophotometer (Micro Drop; Bio-DL). cDNA synthesis was performed using PrimeScript RT Reagent Kit (cat. no. RR037A; Takara Bio, Inc.) under the following conditions: 37˚C for 15 min, 85˚C for 5 sec. qPCR was performed using PowerTrack™ SYBR Green Master Mix (Thermo Fisher Scientific, Inc.) and specific primers as follows: inducible nitric oxide synthase (iNOS) forward, 5'-TCCTGGACATTACGACCCCT-3' and reverse, 5'-AGGCCTCCAATCTCTGCCTA-3'; IL-12 forward, 5'-CTCCTGTGGGAGAAGCAGAC-3' and reverse, 5'-CAGATAGCCCATCACCCTGT-3'; arginase 1 (Arg1) forward, 5'-AGATTATCGGAGCGCCTTTCT-3' and reverse, 5'-CGTGGTCTCTCACGTCATACT-3'; IL-10 forward, 5'-CCAAGCCTTATCGGAAATGA-3' and reverse, 5'-TTTTCACAGGGGAGAAATCG-3'; and GAPDH forward, 5'-GTGTTCCTACCCCCAATGTGT-3' and reverse, 5'-ATTGTCATACCAGGAAATGAGCTT-3'. The PCR cycling conditions were 95˚C for 5 min, followed by 40 cycles of 95˚C for 10 sec and 60˚C for 30 sec. A melting curve analysis was performed at the end. Relative gene expression was calculated using the $2^{-\Delta\Delta Cq}$ method (23). GAPDH was used as the internal reference gene.

Immunofluorescence (IF) staining. IF staining of CD80, CD86, CD206 and CD163 was performed to assess changes in macrophage polarization. After 24 h of cell culture, cells were washed twice with phosphate-buffered saline and fixed with 4% paraformaldehyde (cat. no. A0001; Sangon Biotech Co., Ltd.) for 20 min at room temperature. Cells were then permeabilized with 0.1% Triton X-100 (cat. no. A600413; Sangon Biotech Co., Ltd.) for 10 min, followed by blocking with 5% normal goat serum (cat. no. C0265; Beyotime Institute of Biotechnology) for 1 h at room temperature. Subsequently, cells were incubated overnight at 4˚C with the following primary antibodies: CD80 (1:200; cat. no. 66406-1-Ig), CD86 (1:200; cat. no. 13395-1-AP), CD206 (1:200; cat. no. 83485-1-RR) and CD163 (1:200; cat. no. 16646-1-AP; all from Proteintech Group, Inc.). The next day, cells were washed three times with PBS and incubated for 1 h at room temperature with Alexa Fluor 488-conjugated secondary antibody (1:1,000;

cat. no. A11034) and Alexa Fluor 594-conjugated secondary antibody (1:1,000; cat. no. A11032; both from Thermo Fisher Scientific, Inc.). Nuclei were stained with 1 μg/ml DAPI (cat. no. C1002; Beyotime Institute of Biotechnology) for 10 min, and images were captured using a fluorescence microscope (IX71; Olympus Corporation).

Flow cytometric analysis of macrophage polarization. Macrophage polarization was further quantified by flow cytometry. After the indicated treatments, RAW264.7 cells were collected, washed with PBS, and incubated with fluorochrome-conjugated anti-mouse antibodies against CD80-FITC (cat. no. 104705), CD86-PE (cat. no. 105007), CD206-PerCP/Cyanine5.5 (cat. no. 141715) and CD163-APC (cat. no. 155305; all from BioLegend, Inc.) according to the manufacturers' instructions. After incubation in the dark at 4˚C for 30 min, cells were washed twice with PBS and analyzed using a BD Accuri C6 flow cytometer (BD Biosciences). Debris and doublets were excluded by forward- and side-scatter gating, and at least 10,000 events were acquired for each sample. The percentages of CD80/CD86-positive and CD206/CD163-positive cells were analyzed using FlowJo software (v10.8; BD Biosciences).

Experimental animals. Male C57BL/6 mice (7-8 weeks old, 20-25 g) were obtained from Hunan Silaike Jingda Laboratory Animal Co., Ltd. [production license No. SCXK (Xiang) 2019-0004]. Only male mice were used in this initial *in vivo* experiment to reduce variability associated with sex-dependent immune and hormonal differences and because previous LPS/endotoxemia studies have reported sex-dependent inflammatory and organ-injury responses, with male mice often showing greater susceptibility or more pronounced injury than female mice (24). All animal experiments were conducted at the Guangxi University of Chinese Medicine, which holds the laboratory animal use license No. SYXK [Gui] 2019-0001. All procedures were approved by the Animal Ethics Committee of Guangxi University of Chinese Medicine (approval no. DW20240923-01; Nanning, China). Animals were housed in a controlled environment (25±2˚C, 65% humidity, 12/12-h light/dark cycle) with free access to standard chow and purified water. All animal procedures complied with the ARRIVE guidelines (25) and the National Institutes of Health Guide for the Care and Use of Laboratory Animals.

Establishment of the LPS-induced systemic inflammation model and pretreatment regimen. Mice were randomly assigned to the following groups: control, LPS model, TPLA (low, medium and high dose) and DEX (n=6 per group). A total of 36 mice were used in the *in vivo* experiment, with six mice allocated to each group. All 36 animals completed the experimental protocol and were included in the final analysis. No animals were excluded, no animals were found dead, and no premature euthanasia was required during the study. At the scheduled endpoint, all 36 mice were euthanized for sample collection. TPLA was administered orally at 50, 100, or 200 mg/kg once daily for 27 consecutive days as a pretreatment regimen (11). The DEX group received DEX at 1 mg/kg (26). On the last two days of the experiment, mice were challenged with intraperitoneal LPS (20 mg/kg), twice daily for two consecutive days, to induce acute systemic inflammatory injury (27). Mice exhibiting lethargy, piloerection and labored breathing within 24 h were considered successfully modeled (28). Core body temperature was measured 6 h after the final LPS injection. The total duration of the *in vivo* experiment was 27 days, and mice were euthanized 6 h after the final LPS injection on day 27. At the scheduled endpoint, mice were deeply anesthetized and euthanized by intraperitoneal injection of 1% sodium pentobarbital solution (10 mg/ml; Sigma-Aldrich, P3761) at 150 mg/kg body weight (29,30), followed by cervical dislocation as a secondary physical method. Death was verified by the absence of spontaneous respiration and heartbeat, loss of corneal and pedal withdrawal reflexes, and absence of response to toe pinch before tissue collection. Humane endpoints were defined before the experiment to minimize animal suffering. Animals were monitored at least twice daily for signs of distress, including persistent lethargy, severe weight loss (>20% of body weight), hypothermia, hunched posture, tremors, unresponsiveness, or labored breathing. Mice showing any of these signs would have been immediately euthanized using the same sodium pentobarbital protocol.

Hematoxylin and eosin (H&E) staining. Lung and liver tissues were collected and fixed in 10% neutral-buffered formalin (cat. no. HT501128; MilliporeSigma) for 24 h at room temperature. After dehydration, clearing and paraffin embedding, 4 μm-thick sections were cut using a microtome (cat. no. RM2255; Leica Biosystems). Sections were deparaffinized using xylene (X5; MilliporeSigma) and rehydrated through graded ethanol. Hematoxylin (cat. no. GHS132) and eosin (cat. no. E4003; both from MilliporeSigma) were used for nuclear and cytoplasmic staining, respectively. After dehydration and clearing, slides were mounted with neutral resin (cat. no. G8110; MilliporeSigma) and examined under a light microscope (BX53; Olympus Corporation). Semi-quantitative histopathological scoring was performed to evaluate lung and liver injury. For each animal, representative non-overlapping fields were observed, and the overall pathological injury was scored by two independent investigators blinded to the experimental groups. Lung injury was assessed according to alveolar structural destruction, alveolar septal thickening, inflammatory cell infiltration, congestion and alveolar collapse. Liver injury was assessed according to hepatocellular swelling, cytoplasmic rarefaction, inflammatory cell infiltration, nuclear pyknosis and disruption of hepatic cord architecture. The severity of pathological injury was graded using a 0-4 scale as follows: 0, no obvious injury; 1, mild injury; 2, moderate injury; 3, severe injury; and 4, very severe injury.

Statistical analysis. Statistical analyses and graph generation were performed using GraphPad Prism 10.0 (GraphPad Software; Dotmatics). Data are presented as the mean ± standard deviation. Semi-quantitative histopathological injury scores are presented as median with interquartile range. Data normality was assessed using the Shapiro-Wilk test. For normally distributed data, independent-samples t-tests were used for two-group comparisons, and one-way ANOVA with Tukey's post hoc test was used for multiple group comparisons.

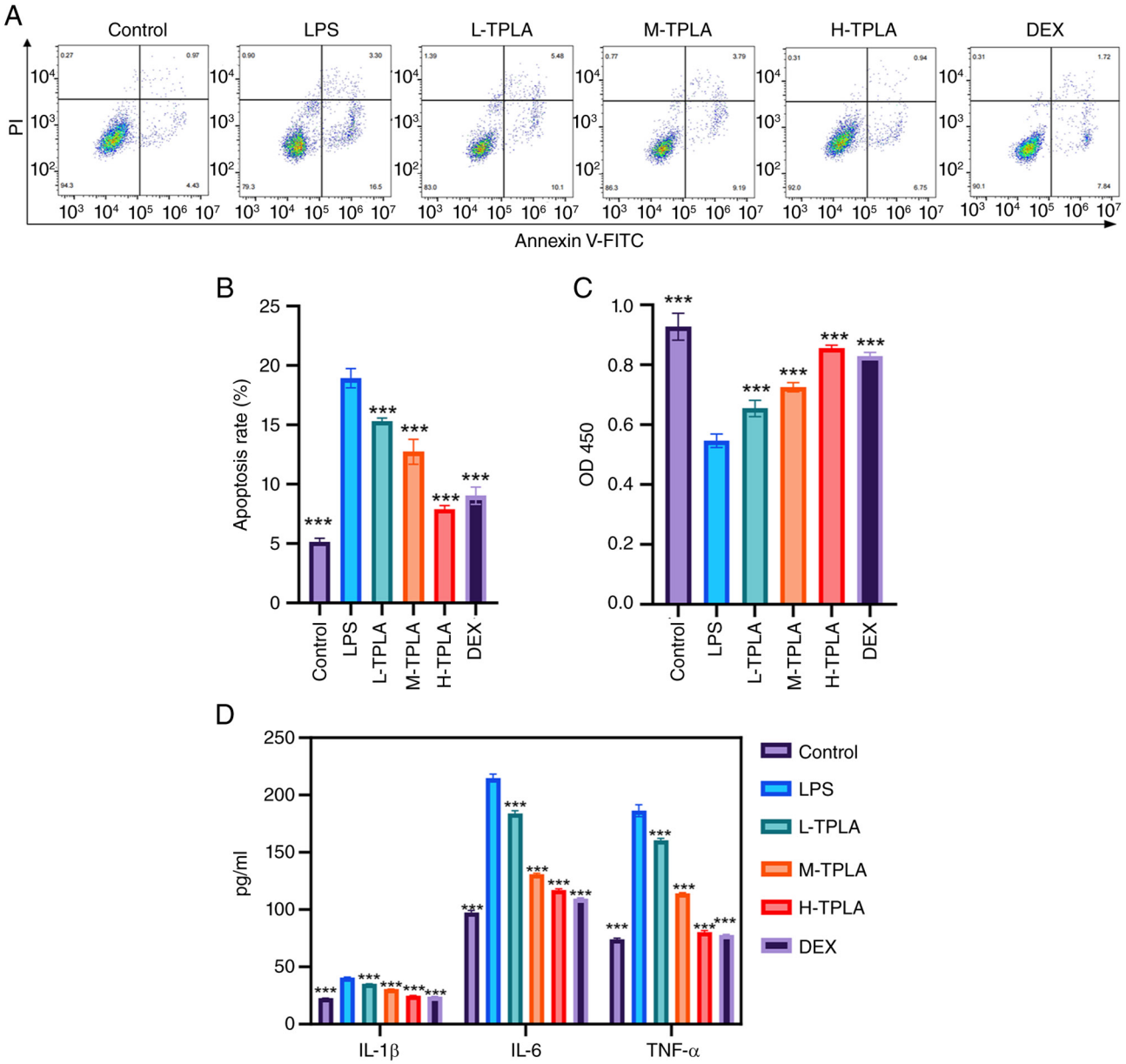

Figure 1. TPLA attenuates LPS-induced apoptosis and pro-inflammatory cytokine production in macrophages. (A) Representative flow cytometry histograms of apoptotic cells. (B) Quantification of apoptotic cell percentage. (C) Cell viability determined by CCK-8 assay. (D) Concentrations of IL-1β, IL-6 and TNF-α in cell supernatants measured by ELISA. Data were analyzed by one-way ANOVA followed by Tukey's post hoc test. Data are presented as mean ± SD (n=3). ***P<0.001 compared with the LPS group. TPLA, total phenolics from *Laggera alata*; LPS, lipopolysaccharide; DEX, dexamethasone; CCK-8, Cell counting kit-8; ELISA, Enzyme-linked immunosorbent assay.

For non-normally distributed data, the Wilcoxon rank-sum test and Kruskal-Wallis test with Dunn's multiple comparisons were applied. P<0.05 was considered to indicate a statistically significant difference.

Results

TPLA significantly alleviates LPS-induced macrophage apoptosis and pro-inflammatory cytokine release. Flow cytometric analysis revealed a significant increase in both early and late apoptotic rates in macrophages treated with LPS, whereas treatment with low, medium and high doses of TPLA reduced apoptosis in a dose-dependent manner, with the high-dose group showing an effect similar to that of DEX (Fig. 1A). Quantitative analysis confirmed that the apoptotic rate in the LPS group increased to ~20%, while treatment with TPLA reduced this rate to ~15, 13 and 8%, respectively, and these reductions were statistically significant compared with the LPS group (Fig. 1B). Cell viability assessed by CCK-8 assay showed a significant reduction following LPS stimulation, which was restored in a dose-dependent manner by TPLA treatment to levels approaching those of the control group (Fig. 1C). ELISA results demonstrated that LPS significantly increased the levels of IL-1β, IL-6 and TNF-α, while TPLA treatment significantly suppressed the secretion of these cytokines, especially in the high-dose group, which exhibited cytokine levels comparable to the control (Fig. 1D).

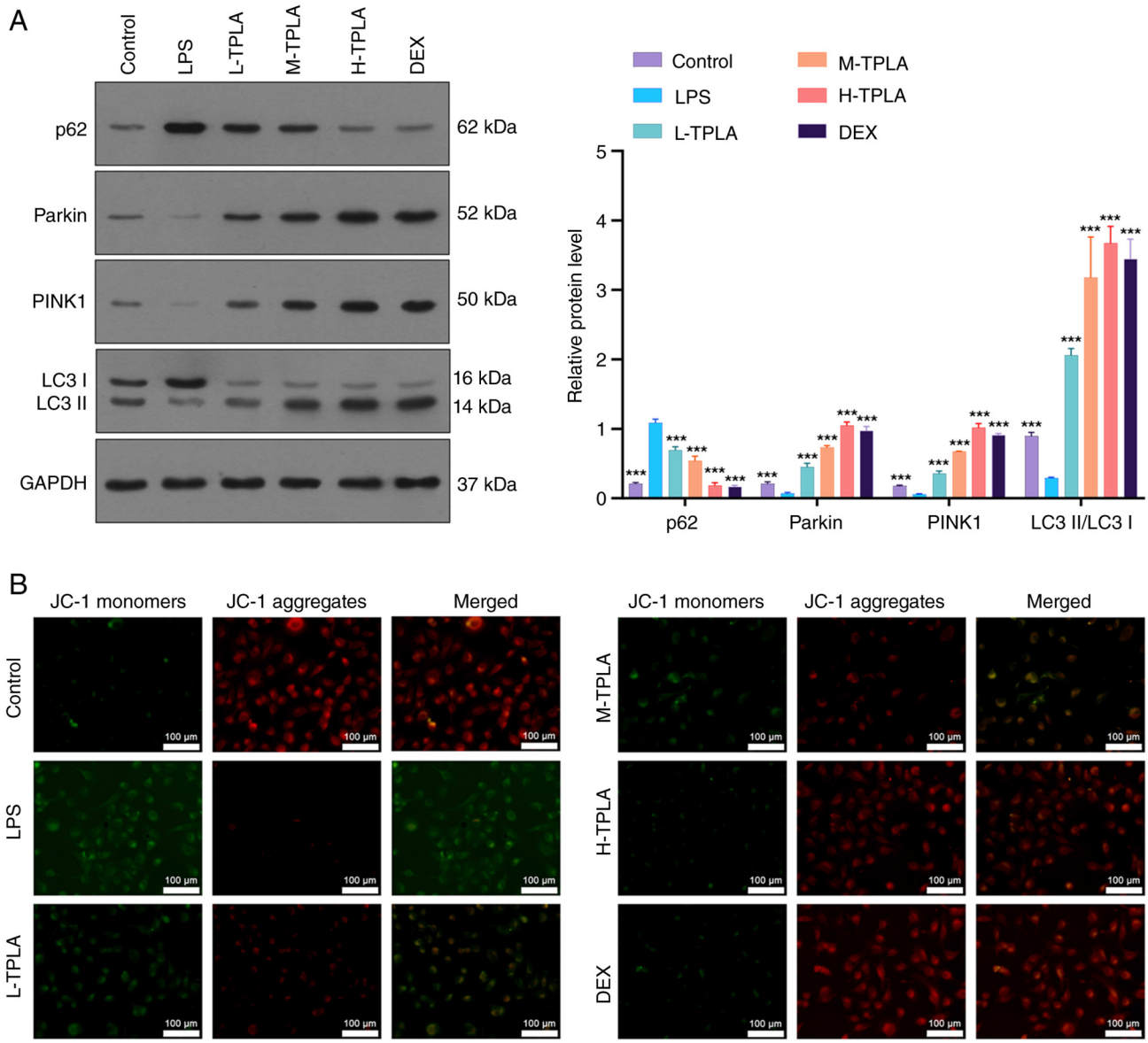

Figure 2. TPLA restores LPS-suppressed PINK1/Parkin-associated mitophagy-related signaling in macrophages. (A) Western blot analysis of p62, Parkin, PINK1 and LC3 protein levels. (B) JC-1 staining to evaluate mitochondrial membrane potential (ΔΨm). Scale bar, 100 μm. Data were analyzed by one-way ANOVA followed by Tukey's post hoc test. Data are presented as the mean ± SD (n=3). ***P<0.001 compared with the LPS group. The protein levels of p62, Parkin and PINK1 were normalized to GAPDH, whereas LC3 was expressed as the LC3-II/LC3-I ratio. TPLA, total phenolics from *Laggera alata*; LPS, lipopolysaccharide; DEX, dexamethasone.

TPLA restores LPS-suppressed PINK1/Parkin-associated mitophagy-related signaling in macrophages. Western blot analysis indicated that LPS treatment significantly reduced LC3-II expression and decreased the LC3-II/LC3-I ratio, suggesting suppression of autophagy-related activity. This impairment was reversed by medium and high doses of TPLA, which restored the LC3-II/LC3-I ratio to levels comparable to those in the DEX group. In addition, LPS elevated expression of the autophagy substrate p62 while downregulating the mitophagy-related proteins Parkin and PINK1. TPLA treatment dose-dependently reduced p62 expression and significantly increased Parkin and PINK1 levels, consistent with activation of PINK1/Parkin-associated mitophagy-related signaling (Fig. 2A). JC-1 staining revealed that LPS reduced MMP, as evidenced by increased green monomer fluorescence and decreased red aggregate fluorescence. This mitochondrial dysfunction was reversed by TPLA treatment, particularly at higher doses (Fig. 2B).

TPLA suppresses LPS-induced M1 macrophage polarization and promotes M2 phenotype transition. RT-qPCR analysis showed that LPS stimulation significantly increased M1-associated genes iNOS and IL-12, while decreasing M2-associated genes Arg1 and IL-10. TPLA treatment dose-dependently reversed this trend, decreasing iNOS and IL-12 expression and enhancing Arg1 and IL-10 expression (Fig. 3A). ELISA results demonstrated that LPS significantly elevated levels of M1-associated cytokines IL-1α and IL-1β and suppressed M2-associated cytokines IL-4 and IL-10. TPLA treatment decreased M1 cytokine levels and increased M2 cytokine levels in a dose-dependent manner (Fig. 3B). IF analysis further confirmed these results. CD80/CD86

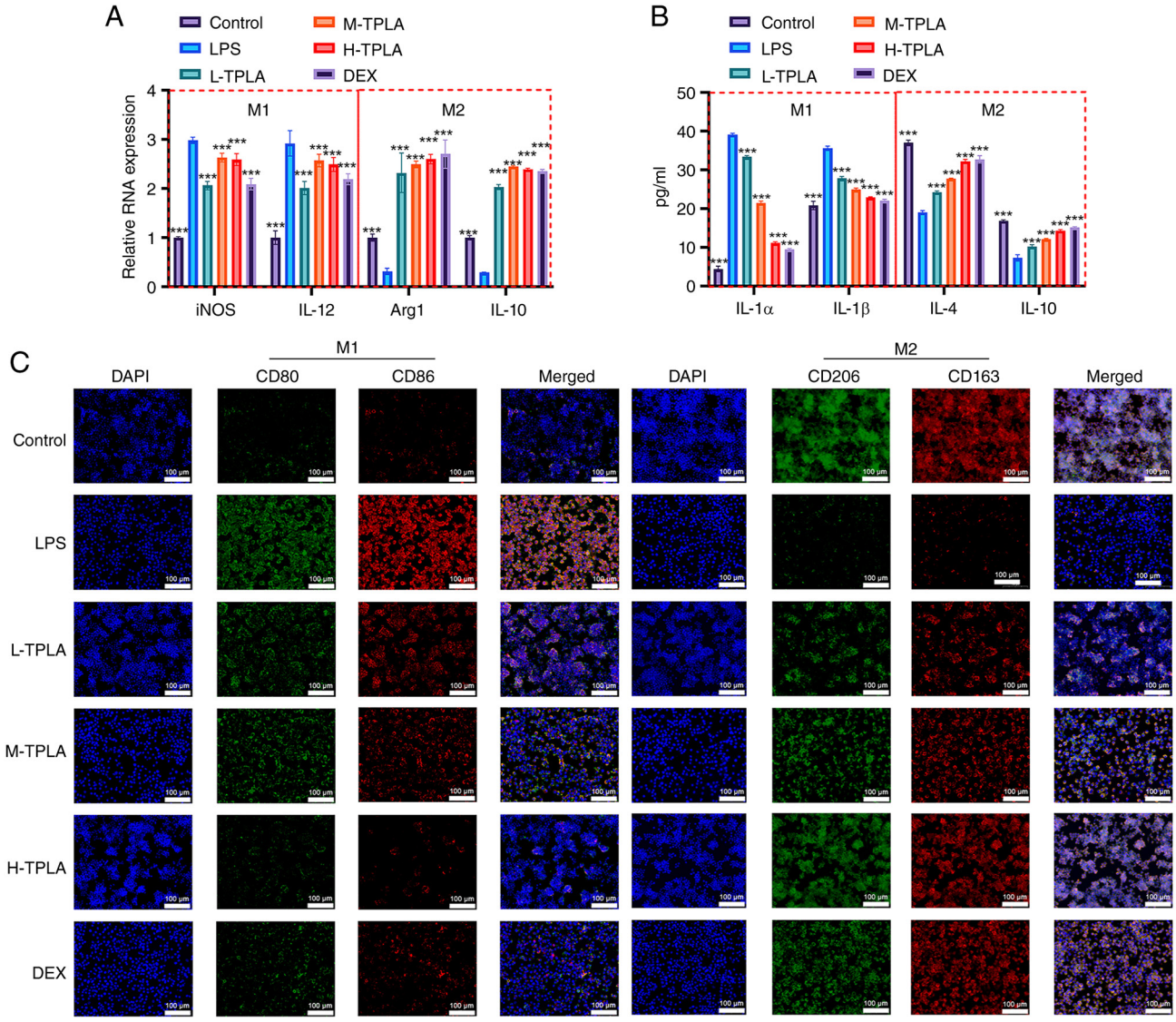

Figure 3. TPLA suppresses LPS-induced M1-like macrophage polarization. (A) Reverse transcription-quantitative PCR analysis of M1 markers (iNOS and IL-12) and M2 markers (Arg1 and IL-10). (B) ELISA quantification of M1 cytokines (IL-1α and IL-1β) and M2 cytokines (IL-4 and IL-10). (C) Immunofluorescence staining of M1 markers (CD80 and CD86) and M2 markers (CD206 and CD163). Scale bar, 100 μm. Data were analyzed by one-way ANOVA followed by Tukey's post hoc test. Data are presented as the mean ± SD (n=3). ***P<0.001 compared with the LPS group. TPLA, total phenolics from *Laggera alata*; LPS, lipopolysaccharide; iNOS, inducible nitric oxide synthase; DEX, dexamethasone.

expression (M1 markers) was increased in the LPS group, while CD206/CD163 expression (M2 markers) was reduced. TPLA treatment reversed these changes, with high-dose TPLA showing effects comparable to DEX (Fig. 3C). Flow cytometric analysis further confirmed the regulatory effect of TPLA on macrophage polarization. LPS stimulation significantly increased the proportion of CD80/CD86-positive M1 macrophages compared with the control group, whereas TPLA treatment reduced the CD80/CD86-positive population in a dose-dependent manner. In particular, high-dose TPLA decreased the proportion of CD80/CD86-positive macrophages to a level close to that observed in the DEX group (Fig. 4A). Conversely, LPS significantly decreased the proportion of CD206/CD163-positive M2 macrophages, while TPLA treatment dose-dependently restored the CD206/CD163-positive population. The effect of high-dose TPLA was comparable to that of DEX (Fig. 4B).

TPLA shifts macrophage polarization toward an M2-like phenotype and enhances PINK1/Parkin-associated mitophagy-related signaling. LPS stimulation significantly increased the proportion of CD80/CD86-positive M1 macrophages compared with the control group, whereas high-dose TPLA treatment reduced the CD80/CD86-positive population (Fig. 5A). Conversely, LPS significantly decreased the proportion of CD206/CD163-positive M2 macrophages, while high-dose TPLA treatment restored the CD206/CD163-positive population (Fig. 5B). However, co-treatment with Mdivi-1 partially reversed the effects of high-dose TPLA. To further examine whether the mitophagy-related effects of TPLA were associated with the PINK1/Parkin pathway, Mdivi-1 was used to inhibit mitochondrial fission- and mitophagy-related responses. Western blot analysis demonstrated that high-dose TPLA increased the expression levels of Parkin and PINK1, enhanced the LC3-II/LC3-I ratio, and reduced

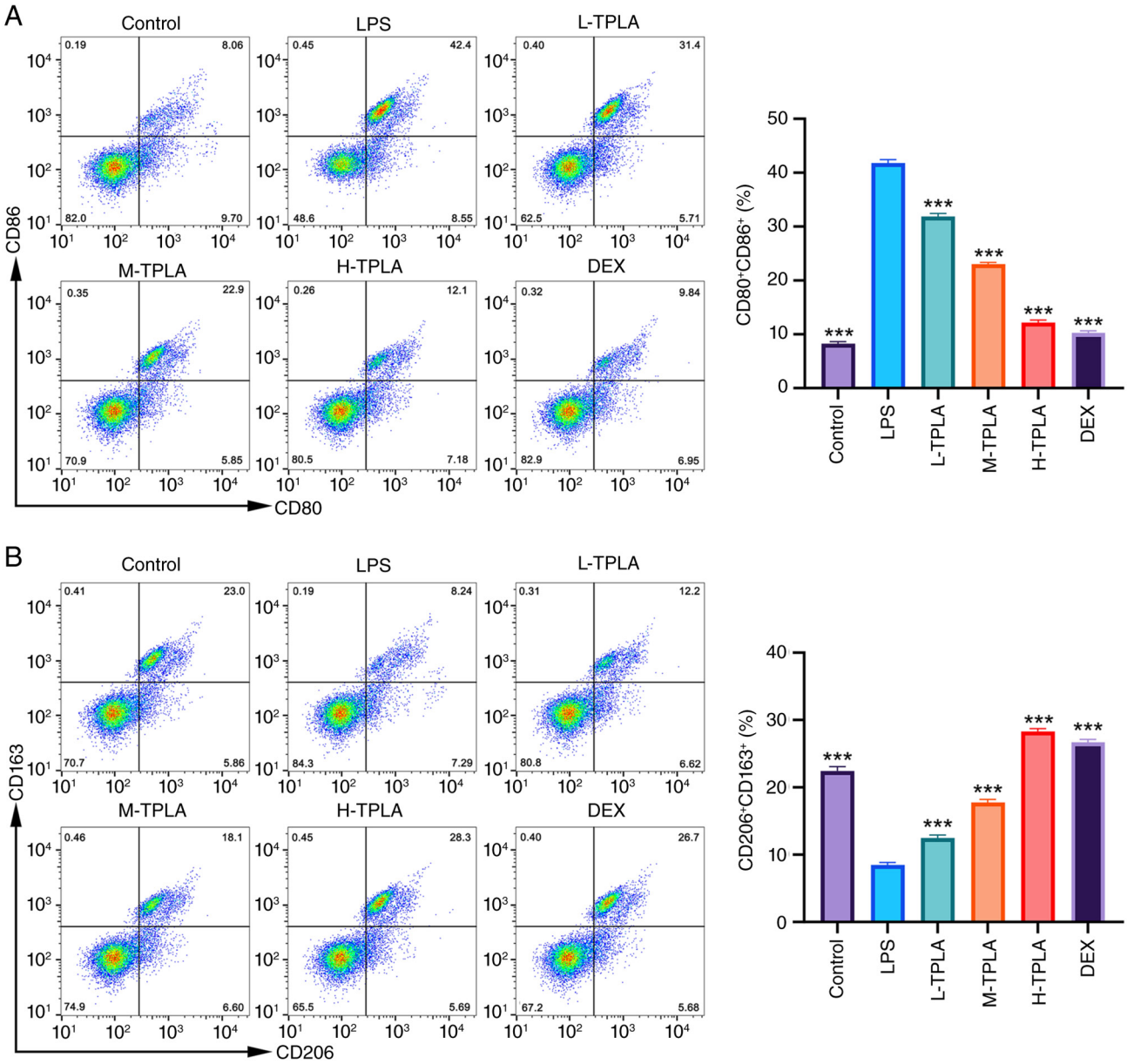

Figure 4. TPLA shifts macrophage polarization toward an M2-like phenotype. (A) Representative flow cytometry plots and quantification of CD80/CD86-positive M1 macrophages. (B) Representative flow cytometry plots and quantification of CD206/CD163-positive M2 macrophages. Data were analyzed by one-way ANOVA followed by Tukey's post hoc test. Data are presented as the mean ± SD (n=3). ***P<0.001 compared with the LPS group. TPLA, total phenolics from *Laggera alata*; LPS, lipopolysaccharide; L-TPLA, low-dose TPLA; M-TPLA, medium-dose TPLA; H-TPLA, high-dose TPLA; DEX, dexamethasone.

p62 accumulation compared with the LPS group. However, co-treatment with Mdivi-1 partially reversed these changes, as evidenced by decreased Parkin and PINK1 expression, reduced LC3-II/LC3-I ratio, and increased p62 expression (Fig. 5C). These results indicate that TPLA-induced activation of the PINK1/Parkin-associated mitophagy pathway was partially attenuated by Mdivi-1.

TPLA alleviates lung and liver tissue injury in an LPS-induced systemic inflammation mouse model. H&E staining of lung tissues revealed that the control group exhibited normal alveolar architecture with thin alveolar septa and minimal inflammatory cell infiltration. By contrast, the LPS group displayed marked pathological injury, characterized by alveolar collapse, interstitial thickening, congestion, and marked inflammatory cell infiltration. Semi-quantitative histopathological scoring further confirmed that the lung injury score was markedly increased in the LPS group compared with the control group. TPLA treatment reduced lung pathological injury in a dose-dependent manner, with the medium- and high-dose groups showing clear attenuation of alveolar structural disruption and inflammatory infiltration. The effect of high-dose TPLA was similar to that observed in the DEX group (Fig. 6A and B). In liver tissues, the control group demonstrated orderly hepatic cords, clear hepatic sinusoidal structures and intact hepatocyte morphology. The LPS group exhibited pronounced hepatocellular swelling, cytoplasmic rarefaction, inflammatory infiltration and nuclear pyknosis. Semi-quantitative scoring showed that LPS markedly increased the liver injury score, whereas TPLA treatment

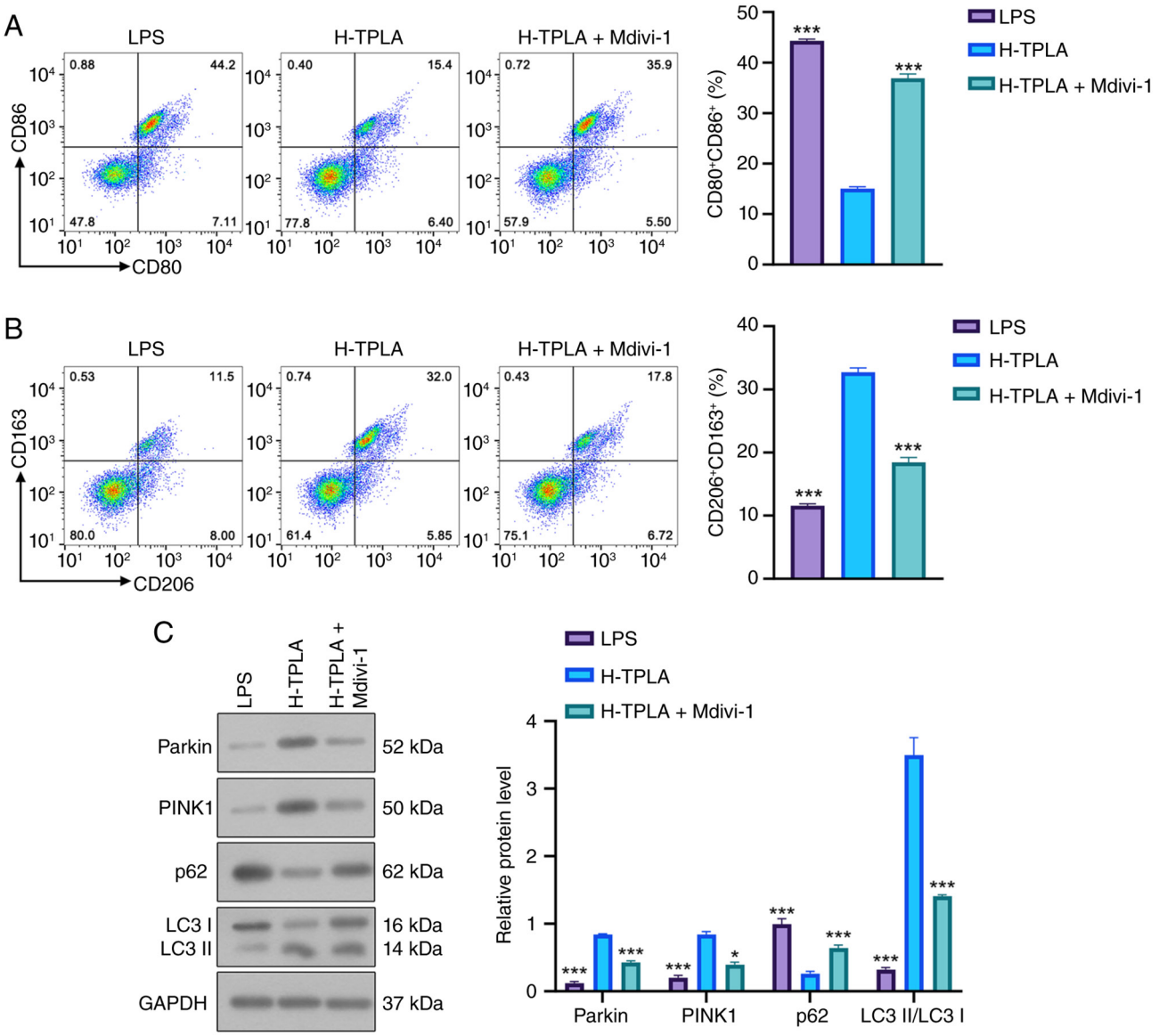

Figure 5. TPLA shifts macrophage polarization toward an M2-like phenotype and enhances PINK1/Parkin-associated mitophagy-related signaling. (A) Representative flow cytometry plots and quantification of CD80/CD86-positive M1 macrophages. (B) Representative flow cytometry plots and quantification of CD206/CD163-positive M2 macrophages. (C) Western blot analysis and quantitative analysis of Parkin, PINK1, p62 and the LC3-II/LC3-I ratio in macrophages treated with LPS, H-TPLA, or H-TPLA + Mdivi-1. Data were analyzed by one-way ANOVA followed by Tukey's post hoc test. Data are presented as the mean ± SD (n=3). *P<0.05 and ***P<0.001 compared with the H-TPLA group. The protein levels of p62, Parkin and PINK1 were normalized to GAPDH, whereas LC3 was expressed as the LC3-II/LC3-I ratio. TPLA, total phenolics from *Laggera alata*; LPS, lipopolysaccharide; H-TPLA, high-dose TPLA; Mdivi-1, mitochondrial division inhibitor 1.

reduced hepatic pathological damage in a dose-dependent manner. In particular, medium- and high-dose TPLA significantly improved hepatocellular architecture and reduced inflammatory changes, with high-dose TPLA showing an effect comparable to DEX (Fig. 6C and D).

TPLA mitigates LPS-induced hypothermia and systemic inflammatory response. LPS administration markedly reduced rectal temperature in mice by ~2˚C compared with the control group. Medium- and high-dose TPLA treatment significantly restored body temperature to levels comparable with the control and DEX groups, while the low-dose group showed no significant improvement (Fig. 7A). ELISA analysis revealed that LPS markedly increased serum levels of IL-1β, IL-6 and TNF-α, reaching ~400, 1,800 and 800 pg/ml, respectively. TPLA treatment reduced serum levels of these inflammatory cytokines in a dose-dependent manner, with the high-dose group showing the most pronounced effect, comparable to that of DEX (Fig. 7B).

Discussion

Sepsis is a life-threatening systemic inflammatory syndrome caused by infection, often accompanied by immune dysregulation and multi-organ failure (31). In TCM, the pathogenesis of sepsis is attributed to disruptions in qi and blood as well as dysfunction of the internal organs. TCM interventions are considered to alleviate inflammatory damage by modulating systemic immune responses, restoring internal homeostasis and rebalancing the microbiota (32). The present study

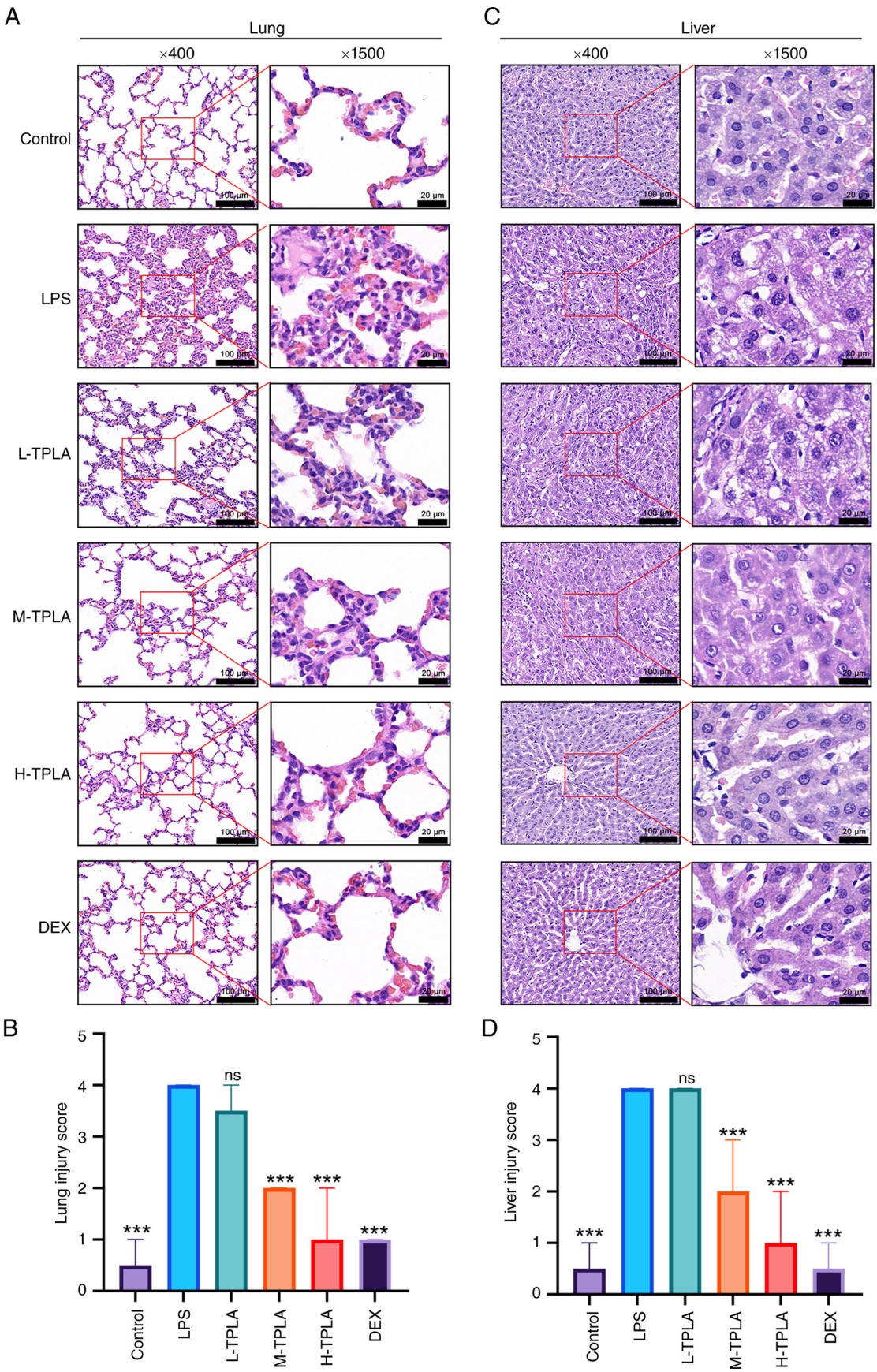

Figure 6. TPLA alleviates lung and liver tissue damage in an LPS-induced systemic inflammation mouse model. (A) Representative H&E-stained images of lung tissues. (B) Semi-quantitative histopathological injury scores of lung tissues. (C) Representative H&E-stained images of liver tissues. (D) Semi-quantitative histopathological injury scores of liver tissues. Scale bar, 100 μm; enlarged, 20 μm. Data are presented as median with interquartile range (n=6). Statistical analysis was performed using the Kruskal-Wallis test followed by Dunn's multiple comparisons test. ***P<0.001 compared with the LPS group. TPLA, total phenolics from *Laggera alata*; LPS, lipopolysaccharide; L-TPLA, low-dose TPLA; M-TPLA, medium-dose TPLA; H-TPLA, high-dose TPLA; DEX, dexamethasone; H&E, hematoxylin and eosin; ns, not significant.

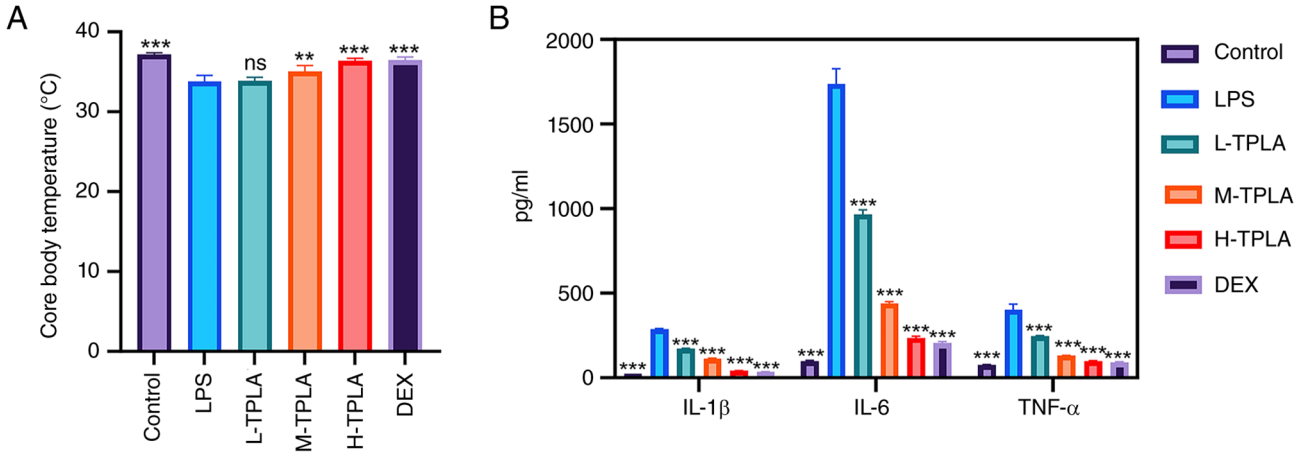

Figure 7. TPLA mitigates LPS-induced hypothermia and systemic inflammation in an LPS-induced systemic inflammation model. (A) Core body temperature of mice measured 6 h after the final LPS injection following the 27-day pretreatment regimen. (B) Serum levels of IL-1β, IL-6 and TNF-α determined by ELISA. Data were analyzed by one-way ANOVA followed by Tukey's post hoc test. Data are presented as the mean ± SD (n=6). **P<0.01 and ***P<0.001 compared with the LPS group. TPLA, total phenolics from *Laggera alata*; LPS, lipopolysaccharide; DEX, dexamethasone.

provides evidence that TPLA attenuates LPS-induced acute inflammatory injury through modulation of mitophagy-related signaling and macrophage polarization (Fig. 8).

Previous studies have demonstrated the immunomodulatory effects of TPLA. Its bioactive constituents have been reported to suppress M1 macrophage markers and enhance M2 polarization, thereby exerting anti-inflammatory effects (11). Other compounds derived from *Laggera alata*, such as isochlorogenic acid A, have shown hepatoprotective and anti-inflammatory activities, particularly by targeting pathways like HMGB1/TLR4/NF-κB in hepatic fibrosis (10). These findings provide a pharmacological foundation for the potential application of TPLA in inflammatory disorders.

Macrophages play a central role in the progression and resolution of sepsis. Although the M1/M2 classification provides a useful framework, recent reviews emphasize that macrophage polarization represents a highly plastic and dynamic spectrum regulated by inflammatory stimuli, metabolic reprogramming, tissue microenvironment and disease stage (33-35). In LPS-induced models, macrophages are driven toward the M1 phenotype, amplifying the inflammatory response (36). Consistently, recent studies on sepsis-associated acute lung injury have shown that macrophage polarization is closely coupled with mitochondrial dysfunction, oxidative stress and metabolic remodeling, further supporting mitochondria-centered regulation as a potential strategy to rebalance inflammatory macrophage responses (17,18). In the present study, TPLA shifted macrophages away from an M1-like phenotype and toward an M2-like phenotype. This immunoregulatory role is consistent with recent evidence showing that natural products or bioactive small molecules can regulate inflammatory injury by targeting mitochondrial dysfunction, mitophagy and macrophage polarization. For example, urolithin A was recently reported to alleviate sepsis-induced acute lung injury by reducing mitochondrial dysfunction, enhancing PINK1/Parkin-associated mitophagy, and modulating macrophage polarization (37). In addition to regulating macrophage polarization, TPLA also mitigated the systemic inflammatory response induced by LPS. One of the early indicators of severe sepsis is hypothermia, which reflects dysregulation of thermoregulation. In the present study, LPS administration significantly reduced the core body temperature of mice, consistent with previous models of sepsis (38,39). TPLA treatment, particularly at medium and high doses, restored body temperature to near-normal levels, comparable to the effect of DEX. This thermoregulatory protection is likely linked to TPLA's ability to inhibit pro-inflammatory cytokines such as IL-1β, IL-6 and TNF-α. As hypothermia in sepsis is associated with poor prognosis, these findings suggest that TPLA may help restore inflammatory and systemic homeostasis in this model.

A key mechanistic insight from the present study is the involvement of mitophagy in TPLA's anti-inflammatory effects. Mitophagy is essential for maintaining mitochondrial integrity, limiting mitochondrial ROS accumulation, and preserving cellular metabolic homeostasis. Recent reviews have highlighted that mitophagy can be mediated by ubiquitin-dependent pathways, particularly the PINK1/Parkin pathway, as well as receptor-mediated and other ubiquitin-independent mechanisms (14,40). In macrophages, mitophagy not only affects mitochondrial quality control and energy metabolism but also participates in phenotype remodeling, with recent studies suggesting that activation of mitophagy can facilitate the transition from a pro-inflammatory M1 phenotype toward a reparative or anti-inflammatory M2-like phenotype under certain inflammatory contexts (17). During mitophagy, PINK1 cooperates with the Parkin RBR E3 ubiquitin protein ligase to target damaged mitochondria for lysosomal degradation (41). It has been shown that PINK1/Parkin-mediated mitophagy alleviates inflammatory responses by removing dysfunctional mitochondria and restoring macrophage function (42). In the present study, TPLA upregulated PINK1 expression and was associated with activation of mitophagy-related signaling. This process was accompanied by downregulation of M1 markers such as iNOS and IL-12 and upregulation of M2 markers including Arg1 and IL-10, thereby modulating macrophage polarization and reducing LPS-induced inflammatory responses.

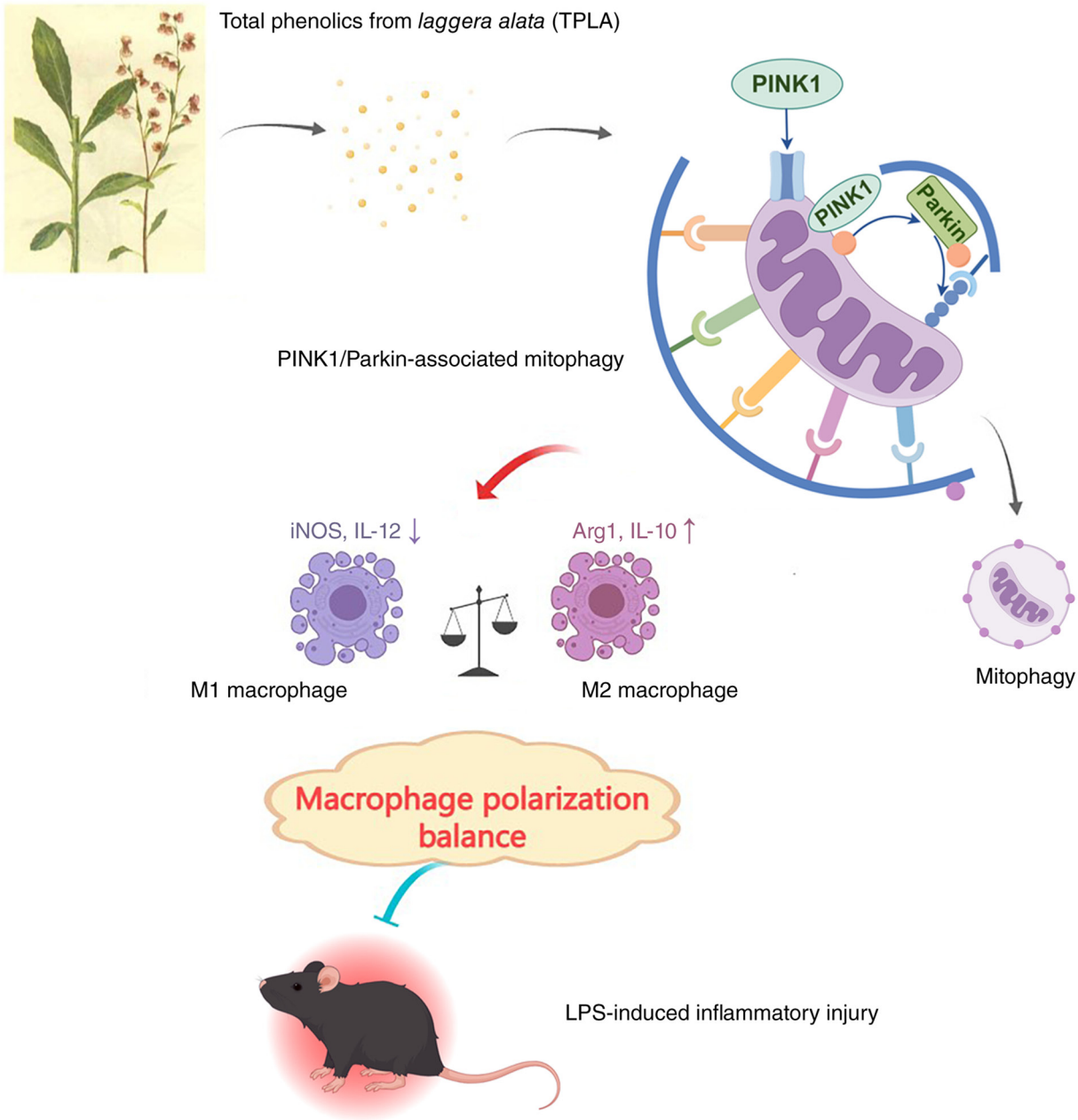

Figure 8. Schematic summary of the proposed mechanism. TPLA activates PINK1/Parkin-associated mitophagy-related signaling and suppresses M1-like macrophage polarization. By restoring the balance of M1/M2 macrophage populations, TPLA helps re-establish immune homeostasis and ameliorates LPS-induced systemic inflammatory injury. The schematic diagram was created using Figdraw. TPLA, total phenolics from *Laggera alata*; iNOS, inducible nitric oxide synthase; LPS, lipopolysaccharide.

Importantly, the additional Mdivi-1 experiment further supported the involvement of PINK1/Parkin-associated mitophagy in the action of TPLA. Mdivi-1 treatment partially reversed the high-dose TPLA-induced increases in Parkin, PINK1 and the LC3-II/LC3-I ratio, and increased p62 accumulation. Together with the flow cytometric evidence showing that TPLA reduced CD80/CD86-positive macrophages and increased CD206/CD163-positive macrophages, these findings suggest that TPLA-mediated macrophage phenotype remodeling is closely associated with activation of the PINK1/Parkin-associated mitophagy pathway.

Following accumulation on damaged mitochondria, PINK1 recruits downstream effectors such as Parkin to initiate mitochondrial ubiquitination and degradation, thus maintaining mitochondrial function (42,43). Dysfunction of mitophagy leads to cellular damage through accumulation of ROS, dysregulated LC3/p62 expression, and reduced adaptability to inflammatory stress (44). The present findings suggest that TPLA alleviated these alterations by enhancing mitophagy-related signaling and improving MMP. PINK1/Parkin-mediated mitophagy has been reported to reduce renal injury by mitigating mitochondrial damage (45), and macrophage mitophagy also protects against renal fibrosis via the PINK1/MFN2/Parkin axis (46). Furthermore, PINK1/Parkin-dependent mitophagy is activated during sepsis and has been shown to exert anti-apoptotic and immunoregulatory effects in dendritic

cells (47). The present study further supports the possibility that TPLA mitigates inflammatory responses through activation of the PINK1/Parkin-associated mitophagy pathway.

Dysregulated mitophagy not only impairs mitochondrial function but also exacerbates macrophage-driven inflammation. It has been previously shown that in the absence of functional mitophagy, macrophages exhibit enhanced inflammatory responses and reduced adaptability to repeated inflammatory stimuli (48). Interestingly, the role of mitophagy in immune regulation is bidirectional. Patoli *et al* (49) found that inhibition of PINK1-dependent mitophagy enhanced macrophage bactericidal activity via mitochondrial ROS and caspase signaling, suggesting context-dependent effects. Qi *et al* (21) proposed that stage-specific modulation of mitophagy may help manage cytokine storms in early sepsis while supporting immune recovery later. The current findings contribute to this framework by highlighting how TPLA modulates mitophagy-related signaling to balance macrophage function and inflammation. Thus, TPLA may exert both anti-inflammatory and immunomodulatory effects through regulation of the PINK1/Parkin-associated pathway.

Nevertheless, although the present study supports the protective potential of TPLA against LPS-induced systemic inflammatory injury, several limitations should be acknowledged. Although the present study provides pharmacological and protein-expression evidence supporting the involvement of PINK1/Parkin-associated mitophagy, direct ultrastructural evidence of mitophagy was not obtained, as transmission electron microscopy was not performed to visualize mitophagosomes or mitochondria-containing autophagic structures. In addition, further studies using genetic loss-of-function approaches, such as PINK1 or Parkin knockdown, will be required to more definitively establish the causal relationship between mitophagy and macrophage polarization. Future studies should integrate morphological validation, mitophagy flux assessment, and genetic intervention to further clarify the mechanism by which TPLA regulates macrophage function in sepsis-related inflammatory injury. In addition, the 27-day oral administration of TPLA was designed as a pretreatment regimen and does not mimic the clinical therapeutic window of established acute sepsis; therefore, the *in vivo* findings should be interpreted as protective effects against LPS-induced systemic inflammatory injury rather than direct therapeutic efficacy in established sepsis. *In vivo* validation of PINK1/Parkin-associated mitophagy and macrophage polarization in lung and liver tissues was not performed and should be addressed in future studies. Another limitation is that only male mice were used in the *in vivo* experiment. Although this design was intended to reduce variability associated with sex-dependent hormonal and immune differences, it may introduce sex-related bias and limit the generalizability of the findings to female animals. Future studies should include both male and female mice and evaluate sex as a biological variable to determine whether the protective effects of TPLA are sex-dependent.

Acknowledgements

Not applicable.

Funding

The present study was supported by Guangxi Natural Science Foundation for Young Scholars (grant no. 2024GXNSFBA010302), the Key Discipline Construction Project of High-Level Traditional Chinese Medicine under the National Administration of Traditional Chinese Medicine-Ethnic Minority Medicine (Zhuang Medicine) (grant no. zyyzdxk-2023165), the Qihuang Project-High-level Talent Team Training Program of Guangxi University of Chinese Medicine (grant no. 202414), the Interdisciplinary Innovation Team Project of Traditional Chinese Medicine in Guangxi (grant no. GZKJ2309), the Three-Year Action Plan for High-Level Talent Team Construction (2023) of Guangxi International Zhuang Medicine Hospital (grant no. GZCX20231203), the 'Qingmiao Project' Talent Cultivation Program of Guangxi International Zhuang Medicine Hospital (grant no. 2022001), the Research Initiation Project of Guangxi International Zhuang Medicine Hospital (grant no. 2023GZYJKT008), the National Veteran Pharmacist Inheritance Studio Construction Project [Issued by the Department of Human Resources and Education, National Administration of Traditional Chinese Medicine (2024); grant no. 255].

Availability of data and materials

The data generated in the present study may be requested from the corresponding author.

Authors' contributions

JW performed the *in vivo* and *in vitro* experiments, developed the methodology, organized the raw experimental data, checked data consistency, conducted the formal analysis and wrote the original draft. WZ developed the methodology, performed the *in vivo* and *in vitro* experiments, and performed data validation. GZ performed software analysis and data visualization, organized and checked the datasets used for statistical analysis and figure preparation, contributed to the interpretation of the analytical results, and critically revised the manuscript for important intellectual content. MH provided resources, assisted with the *in vivo* and *in vitro* experiments, contributed to data acquisition and interpretation, and critically revised the manuscript for important intellectual content. XH conceptualized and supervised the study, conducted project administration, and wrote, reviewed and edited the manuscript. JL acquired funding, conceptualized and supervised the study, developed the methodology, and wrote, reviewed and edited the manuscript. XH and JL confirm the authenticity of all the raw data. All authors have read and approved the final version of the manuscript.

Ethics approval and consent to participate

The present study was approved by the Animal Ethics Committee of Guangxi University of Chinese Medicine (approval no. DW20240923-01; Nanning, China). All animal experiments complied with the ARRIVE guidelines and the National Institutes of Health Guide for the Care and Use of Laboratory Animals.

Patient consent for publication

Not applicable.

Competing interests

The authors declare that they have no competing interests.

References

1. Modugula S, Altenbaugh M, Ivanova M, DuMont T and Arshad H: Sepsis epidemiology, definitions, scoring systems, and diagnostic markers. Crit Care Nurs Q 48: 229-236, 2025.
2. Cheng L, Cao Y, Liu S, Lv L, Zhang J, Bao J, Wang G and Xu P: Unveiling the research advances of sepsis: Pathogenesis, precise intervention and clinical perspective. Int J Surg 111: 6260-6289, 2025.
3. Martin-Loeches I, Singer M and Leone M: Sepsis: Key insights, future directions, and immediate goals. A review and expert opinion. Intensive Care Med 50: 2043-2049, 2024.
4. Chanderraj R, Admon AJ, He Y, Nuppnau M, Albin OR, Prescott HC, Dickson RP and Sjoding MW: Mortality of patients with sepsis administered Piperacillin-tazobactam vs cefepime. JAMA Intern Med 184: 769-777, 2024.
5. Lin SJ, Cheng YY, Chang CH, Lee CH, Huang YC and Su YC: Traditional Chinese medicine diagnosis 'Yang-Xu Zheng': Significant prognostic predictor for patients with severe sepsis and septic shock. Evid Based Complement Alternat Med 2013: 759748, 2013.
6. Wang GC, Li GQ, Geng HW, Li T, Xu JJ, Ma F, Wu X, Ye WC and Li YL: Eudesmane-type sesquiterpene derivatives from *Laggera alata*. Phytochemistry 96: 201-207, 2013.
7. Wu YQ, Li N and Wang MW: Research progress on chemical constituents of Laggera plants in China. Zhongguo Zhong Yao Za Zhi 31: 181-184, 2006 (In Chinese).
8. Zhou CX, Wu DY, Li XP, Wu YH, Zhao J, Dong N, Yu RM, Wei W, Zheng QX, Sun HD, *et al*: Research progress in Laggera medicinal plants. Zhongguo Zhong Yao Za Zhi 31: 1133-1140, 2006 (In Chinese).
9. Getahun T, Sharma V and Gupta N: The genus laggera (Asteraceae)-Ethnobotanical and ethnopharmacological information, chemical composition as well as biological activities of its essential oils and extracts: A Review. Chem Biodivers 16: e1900131, 2019.
10. Liu X, Huang K, Zhang RJ, Mei D and Zhang B: Isochlorogenic Acid A attenuates the progression of liver fibrosis through regulating HMGB1/TLR4/NF-κB signaling pathway. Front Pharmacol 11: 582, 2020.
11. Wei J, Tang Y, Qin S, Ma X, Zhong W, Yang P, Deng Q and Ma J: *Laggera alata* attenuates inflammatory response by regulating macrophage polarization in rheumatoid arthritis mice. Mol Biotechnol 66: 1934-1941, 2024.
12. Li Q, Shi X, Huang H, Gao Q, Sun Q, Meng Y, Niu L, Xie C and Yang C: 5β-hydroxycostic acid from *Laggera alata* ameliorates sepsis-associated acute kidney injury through its anti-inflammatory and anti-ferroptosis effects via NF-κB and MAPK pathways. J Ethnopharmacol 341: 119359, 2025.
13. van der Slikke EC, Star BS, van Meurs M, Henning RH, Moser J and Bouma HR: Sepsis is associated with mitochondrial DNA damage and a reduced mitochondrial mass in the kidney of patients with sepsis-AKI. Crit Care 25: 36, 2021.
14. Wang S, Long H, Hou L, Feng B, Ma Z, Wu Y, Zeng Y, Cai J, Zhang DW and Zhao G: The mitophagy pathway and its implications in human diseases. Signal Transduct Target Ther 8: 304, 2023.
15. Picca A, Faitg J, Auwerx J, Ferrucci L and D'Amico D: Mitophagy in human health, ageing and disease. Nat Metab 5: 2047-2061, 2023.
16. Lu Y, Li Z, Zhang S, Zhang T, Liu Y and Zhang L: Cellular mitophagy: Mechanism, roles in diseases and small molecule pharmacological regulation. Theranostics 13: 736-766, 2023.
17. Yang K, Zhao Q, Sun Y, Lin L and Han X: Mitochondrial immunometabolism in sepsis: Orchestrating macrophage polarization and dysfunction. Eur J Med Res 31: 36, 2025.
18. Huang W, Wang L, Huang Z, Sun Z and Zheng B: Peroxiredoxin 3 has a crucial role in the macrophage polarization by regulating mitochondrial homeostasis. Respir Res 25: 110, 2024.
19. Wang Y, Zhu J, Liu Z, Shu S, Fu Y, Liu Y, Cai J, Tang C, Liu Y, Yin X and Dong Z: The PINK1/PARK2/optineurin pathway of mitophagy is activated for protection in septic acute kidney injury. Redox Biol 38: 101767, 2021.
20. Xie F, Zhou J, Liu B, Zhao L, Lv C, Zhang Q, Yuan L, Sun D and Wei W: Low fluoride regulates macrophage polarization through mitochondrial autophagy mediated by PINK1/Parkin axis. Biomolecules 15: 647, 2025.
21. Qi LY, Xing JX, Ouyang BQ, Li YF and Lei M: Role of mitophagy affecting macrophage polarization in immunomodulationin sepsis and traditional Chinese medicine intervention: A review. Zhongguo Yi Xue Ke Xue Yuan Xue Bao 46: 720-731, 2024 (In Chinese).
22. Reilly B, Tan C, Murao A, Nofi C, Jha A, Aziz M and Wang P: Necroptosis-mediated eCIRP release in sepsis. J Inflamm Res 15: 4047-4059, 2022.
23. Livak KJ and Schmittgen TD: Analysis of relative gene expression data using real-time quantitative PCR and the 2(-Delta Delta C(T)) method. Methods 25: 402-408, 2001.
24. Bojalil R, Ruíz-Hernández A, Villanueva-Arias A, Amezcua-Guerra LM, Cásarez-Alvarado S, Hernández-Dueñas AM, Rodríguez-Galicia V, Pavón L, Marquina B, Becerril-Villanueva E, *et al*: Two murine models of sepsis: Immunopathological differences between the sexes-possible role of TGFβ1 in female resistance to endotoxemia. Biol Res 56: 54, 2023.
25. Percie du Sert N, Hurst V, Ahluwalia A, Alam S, Avey MT, Baker M, Browne WJ, Clark A, Cuthill IC, Dirnagl U, *et al*: The ARRIVE guidelines 2.0: Updated guidelines for reporting animal research. PLoS Biol 18: e3000410, 2020.
26. Chen Y, Chen X and Zhou Q: Different effects of a perioperative single dose of dexamethasone on wound healing in mice with or without sepsis. Front Surg 10: 927168, 2023.
27. Fang H, Wang X, Damarla M, Sun R, He Q, Li R, Luo P, Liu JO and Xia Z: Dimethyl Fumarate protects against lipopolysaccharide-(LPS-) Induced sepsis through inhibition of NF-κB pathway in mice. Mediators Inflamm 2023: 5133505, 2023.
28. Davis FM, Schaller MA, Dendekker A, Joshi AD, Kimball AS, Evanoff H, Wilke C, Obi AT, Melvin WJ, Cavassani K, *et al*: Sepsis induces prolonged epigenetic modifications in bone marrow and peripheral macrophages impairing inflammation and wound healing. Arterioscler Thromb Vasc Biol 39: 2353-2366, 2019.
29. Pang D and Laferriere C: Review of intraperitoneal injection of sodium pentobarbital as a method of euthanasia in laboratory rodents. J Am Assoc Lab Anim Sci 59: 346, 2020.
30. Shomer NH, Allen-Worthington KH, Hickman DL, Jonnalagadda M, Newsome JT, Slate AR, Valentine H, Williams AM and Wilkinson M: Review of rodent euthanasia methods. J Am Assoc Lab Anim Sci 59: 242-253, 2020.
31. Wang XH, Xu DQ, Chen YY, Yue SJ, Fu RJ, Huang L and Tang YP: Traditional Chinese Medicine: A promising strategy to regulate inflammation, intestinal disorders and impaired immune function due to sepsis. Front Pharmacol 13: 952938, 2022.
32. Wen Y, Feng C, Chen W, Chen C, Kuang S, Liu F, Tang Q and Chen M: Effect of traditional Chinese medicine on serum inflammation and efficacy in patients with sepsis: A systematic review and meta-analysis. Ann Palliat Med 10: 12456-12466, 2021.
33. Chen S, Saeed A, Liu Q, Jiang Q, Xu H, Xiao GG, Rao L and Duo Y: Macrophages in immunoregulation and therapeutics. Signal Transduct Target Ther 8: 207, 2023.
34. Luo M, Zhao F, Cheng H, Su M and Wang Y: Macrophage polarization: An important role in inflammatory diseases. Front Immunol 15: 1352946, 2024.
35. Ji Y, Li X, Yao X, Sun J, Yi J, Shen Y, Chen B and Sun H: Macrophage polarization: Molecular mechanisms, disease implications, and targeted therapeutic strategies. Front Immunol 16: 1732718, 2025.
36. Li JM, Li X, Chan LWC, Hu R, Zheng T, Li H and Yang S: Lipotoxicity-polarised macrophage-derived exosomes regulate mitochondrial fitness through Miro1-mediated mitophagy inhibition and contribute to type 2 diabetes development in mice. Diabetologia 66: 2368-2386, 2023.
37. Mohsin M, Zaki A, Tabassum G, Khan S, Ali S, Ahmad T and Syed MA: Urolithin-A supplementation alleviates sepsis-induced acute lung injury by reducing mitochondrial dysfunction and modulating macrophage polarization. Mitochondrion 84: 102047, 2025.
38. Tang Z, Ning Z and Li Z: The beneficial effects of Rosuvastatin in inhibiting inflammation in sepsis. Aging (Albany NY) 16: 10424-10434, 2024.

39. Onishi K, Fu HY, Sofue T, Tobiume A, Moritoki M, Saiga H, Ohmura-Hoshino M, Hoshino K and Minamino T: Galectin-9 deficiency exacerbates lipopolysaccharide-induced hypothermia and kidney injury. Clin Exp Nephrol 26: 226-233, 2022.
40. Yang M, Wei X, Yi X and Jiang DS: Mitophagy-related regulated cell death: Molecular mechanisms and disease implications. Cell Death Dis 15: 505, 2024.
41. Han R, Liu Y, Li S, Li XJ and Yang W: PINK1-PRKN mediated mitophagy: Differences between in vitro and in vivo models. Autophagy 19: 1396-1405, 2023.
42. Su L, Zhang J, Gomez H, Kellum JA and Peng Z: Mitochondria ROS and mitophagy in acute kidney injury. Autophagy 19: 401-414, 2023.
43. Choudhuri S, Chowdhury IH and Garg NJ: Mitochondrial regulation of macrophage response against pathogens. Front Immunol 11: 622602, 2020.
44. Liu B, Cao Y, Wang D, Zhou Y, Zhang P, Wu J, Chen J, Qiu J and Zhou J: Zhen-Wu-Tang Induced mitophagy to protect mitochondrial function in chronic glomerulonephritis via PI3K/AKT/mTOR and AMPK pathways. Front Pharmacol 12: 777670, 2021.
45. Zhang X, Du J, Li B, Huo S, Zhang J, Cui Y, Song M, Shao B and Li Y: PINK1/Parkin-mediated mitophagy mitigates T-2 toxin-induced nephrotoxicity. Food Chem Toxicol 164: 113078, 2022.
46. Bhatia D, Chung KP, Nakahira K, Patino E, Rice MC, Torres LK, Muthukumar T, Choi AM, Akchurin OM and Choi ME: Mitophagy-dependent macrophage reprogramming protects against kidney fibrosis. JCI Insight 4: e132826, 2019.
47. Zhang Y, Chen L, Luo Y, Wang K, Liu X, Xiao Z, Zhao G, Yao Y and Lu Z: Pink1/Parkin-mediated mitophagy regulated the apoptosis of dendritic cells in sepsis. Inflammation 45: 1374-1387, 2022.
48. Orekhov AN, Zhuravlev AD, Vinokurov AY, Nikiforov NG, Omelchenko AV, Sukhorukov VN, Sinyov VV and Sobenin IA: Defective mitophagy impairs response to inflammatory activation of Macrophage-Like cells. Curr Med Chem 32: 111-122, 2025.
49. Patoli D, Mignotte F, Deckert V, Dusuel A, Dumont A, Rieu A, Jalil A, Van Dongen K, Bourgeois T, Gautier T, *et al*: Inhibition of mitophagy drives macrophage activation and antibacterial defense during sepsis. J Clin Invest 130: 5858-5874, 2020.